applied sciences

MDPI

Article

Cooperative Target Enclosing and Tracking Control with Obstacles Avoidance for Multiple Nonholonomic Mobile Robots

Xinghua Li [1], Xiaoping Liu [1], Gang Wang [1,*], Song Han [1], Congling Shi [2,*] and Honglei Che [2]

[1] School of Modern Post, Beijing University of Posts and Telecommunications, Beijing 100876, China; lixinghua0620@163.com (X.L.); liuxp@bupt.edu.cn (X.L.); hansong@bupt.edu.cn (S.H.)
[2] Beijing Key Laboratory of Metro Fire and Passenger Transportation Safety, China Academy of Safety Science and Technology, Beijing 100012, China; sychehonglei@163.com
* Correspondence: wangg58977@163.com (G.H.); shicl@chinasafety.ac.cn (C.S.)

Abstract: This paper investigates the cooperative control problem for a group of autonomous nonholonomic mobile robots, in which the robots are required to collaboratively enclose and track a stationary or moving target in a circular formation. In order to solve the challenging problem that the robots with speed constraints move uniformly to the exact position on the circles centered on the target while avoiding obstacles encountered, a distributed coupling controller scheme consisting of target encircling, phase positioning and spacing assignment, and the avoidance of obstacles is proposed. First, a novel circular motion control law based on the feedback control idea of trajectory tracking is proposed, which guides all robots move to the target-centered circles and maintains the expected distances between the robots and the target. Second, a phase positioning and spacing assignment control law by introducing a nonlinear function is proposed, which can be coupled into the circular motion controller to implement the robots converge to the specified position on the circles. Finally, the obstacles avoidance control law based on artificial potential field only with repulsive force is adopted to ensure each robot effectively avoids obstacles. The rigorous theoretical analysis of the convergence of the proposed controller is given, and then the simulations and experiments are provided to validate the effectiveness and applicability of the proposed control scheme.

Keywords: cooperative control; circular formation; phase positioning; spacing assignment; obstacles avoidance; nonholonomic mobile robots

check for updates

Citation: Li, X.; Liu, X.; Wang, G.; Han, S.; Shi, C.; Che, H. Cooperative Target Enclosing and Tracking Control with Obstacles Avoidance for Multiple Nonholonomic Mobile Robots. *Appl. Sci.* **2022**, *12*, 2876. https://doi.org/10.3390/app12062876

Academic Editors: Jose Machado and Alessandro Gasparetto

Received: 18 January 2022
Accepted: 28 February 2022
Published: 11 March 2022

Publisher's Note: MDPI stays neutral with regard to jurisdictional claims in published maps and institutional affiliations.

Copyright: © 2022 by the authors. Licensee MDPI, Basel, Switzerland. This article is an open access article distributed under the terms and conditions of the Creative Commons Attribution (CC BY) license (https://creativecommons.org/licenses/by/4.0/).

1. Introduction

In recent years, the cooperative control problems of a multi-robot system have generated significant research interest owing to their wide practical applications, such as multi-robot cooperative object transportation [1,2], vehicle or fleet escorting and patrolling [3,4], space and ground exploration [5,6], autonomous searching and rescuing [7,8], cooperative pursuit and surveillance [9,10], and environmental monitoring and sampling [11,12]. A multi-robot system can deal with tasks that are difficult to accomplish with an individual robot.

Cooperative target enclosing and tracking control is one of the most actively studied topics within the coordination control of multi-robot system since with such cooperative missions the robots can benefit from moving in a desired formation with certain geometric shapes [13–16]. In such patterns, circular formation has huge merits to successfully complete the tasks and improve their performance due to its flexible, simple and easily implement properties. More specifically, in the process of intercepting and tracking the moving target, the circular formation can not only complete convergence of the target but also flexibly achieve the target tracking, and the chance of the target being attacked or escaping is greatly reduced. In the process of environmental monitoring and sampling, unmanned aerial vehicle (UAV) swarm systems that form a circular formation can more efficiently observe the specified target from different angles to ensure the comprehensiveness and integrity of the sampling process. According to whether a multi-agent system needs to rotate around the target, we usually divide the circular formation into two categories: cooperative circumnavigation and cooperative following.

For the former, cooperative circumnavigation is that a group of autonomous robots circumnavigate the stationary or moving target with prescribed radius, circular velocity, and inter-robot angular spacing [17]. Currently, many circumnavigation-control strategies have been devoted in the most of literature to a single or a team of agents. In [18], a nonlinear periodic continuous time control law based on distance measurement was proposed, which achieved the objective for an agent rotating around a target. In [19], the same circumnavigation problem has been considered by bearing-only measurements to address a surveillance problem, in which a nonholonomic robot achieved a circular motion around a target. However, the forward speed of the agent is required to be a constant, which is easily limited in the practical application. Likewise, a novel bearing-only measurement control scheme was proposed for a single and a group of autonomous nonholonomic mobile robots to enclose around a target of interest [20]. Since the preset target is assumed to be static, this control scheme cannot be applied to the dynamic target situation. To solve this problem, a cooperative controller in Frenet–Serret coordinate system was developed for multiple nonholonomic vehicles via local measurements [21]. However, this controller can only ensure that all robots are evenly distributed on a common circle around a target with time-varying velocity. In [22], a cooperative circumnavigation control methodology based on graph theory and backstepping method was proposed to achieve multiple nonholonomic robots revolving around a moving target. However, the target's speed was only considered in the case of constant speed. In [23], a spacing-adjustment-control strategy was studied, which can make all agents converge to prescribed angular spacing. However, the limitation of the proposed control strategy is that all agents are constrained to move in the one-dimensional space of a circle, i.e., it is completely based on the assumption that the agents are pre-placed on a common circle. Then, the research group proposed a circle formation control method based on the idea of limit-cycle design acting on the double integrator dynamic model [24]. The designed controller is much more universal because all the desired angular spacings between neighboring agents and the desired distances between each agent and the target are equal nor the requirement. However, only the problem of collision avoidance between agents was considered, and the fact that there may be other obstacles in the actual environment was ignored.

For the latter, cooperative following generally addresses some specific missions that do not need to rotate around the goal for energy saving or other practical purposes, such as escorting mission of ships to fleets, and UAVs constantly monitoring specific areas at the specified locations. Similarly, some control strategies have been proposed for cooperatively following a target or an area of interest by a group of agents. In [25], a centralized control algorithm based on the null-space-based behavioral (NSB) control approach has been proposed to deal with the problem of entrapping and escorting an autonomous target by a multi-robot system. The proposed solution was structurally robust to the loss of the vehicles. Similarly, the NSB control method has been defined common tasks in [26], and the Lyapunov theory was used to analyze their stability. For the escorting mission of Euler–Lagrange systems, Gao et al. [27] has structured an outer-inner loop control framework, in which the outer loop considered obstacles, made use of a NSB control architecture and the inner loop applied the adaptive proportional derivative sliding mode control (APD-SMC) law to improve convergence speed and robustness. However, the algorithms required that all robots were evenly distributed on the surface of a sphere or circle and maintained the same specified distance with respect to the target and thus are not suitable for many complex environments and tasks.

However, most aforementioned references assume that the target is in a single state of motion instead of all possible motion states; the robots are used to achieve a circular formation on the same circle and evenly distribute on the common circle. In addition, the obstacles avoidance problem of circular formation added, which includes adjacent agents and surrounding obstacles, is rarely considered. Knowing how to integrate the obstacles avoidance algorithm into the circular formation while ensuring the stability of the formation is also a challenge. In this paper, we study the general following control problem in which a team of nonholonomic mobile robots with speed constraints can form desired circular formations with different circle radii and different angle distances to enclose and track a stationary or moving target. The main contributions of the work can be summed up in three aspects:

1. A novel circular motion control law based on the idea of circular trajectory tracking control is proposed in order to guide multiple nonholonomic mobile robots to converge onto the prescribed circles added with the same or different radii around a static or moving target. On the whole, the designed control law is not only simple and effective, but also can ensure that multiple robots at any initial locations in a plane quickly form the desired circular formation.
2. A phase positioning and spacing adjustment control law has been taken into account by introducing a nonlinear function, maintaining the desired angular spacing from its front neighbors and fixed-phase of the robots on the circles. Hence, by combining it with the circular motion controller, the robots can move to the arbitrary position of the circles given by the user.
3. To solve the obstacles avoidance problem of the multi-robot system in the practical environment, the most well-known artificial potential field method, only with the repulsive force, is adopted to ensure quick obstacles avoidance for each single robot.

The remainder of the paper is organized as follows. In Section 2, the problem formulation is formulated and some useful preliminary results are given. In Section 3, we propose the circular formation controller with obstacles avoidance for multi-robot system to cooperatively enclose and track a stationary or moving target, and its convergence is also analyzed in detail. In Section 4, many simulation and experimental results are provided. Lastly, conclusions are given in Section 5.

Notation: $\mathbb{R}$, $\mathbb{R}^n$, $\mathbb{R}^+$ and $\mathbb{R}^{n\times m}$ denote the set of real numbers, n-dimensional real numbers, positive real numbers, and $n \times m$-dimensional real numbers, respectively. $\mathbb{N}$ and $\mathbb{N}^n$ denote the set of natural numbers and n-dimensional natural numbers. For a matrix $\boldsymbol{A}$, $\boldsymbol{A}^T$ and $\|\boldsymbol{A}\|$ denote its transpose and Euclidean norm, respectively. $\mathbf{0}$ denotes a matrix of zeros.

2. Problem Formulation

Considering a multi-robot system composed of n ($n \geq 2$) nonholonomic mobile robots, the kinematics model of robot i ($i = 1, 2, \ldots, n$) with pure rolling and non-slipping can be described as follows:

$$\dot{x}_i = v_i \cos\theta_i, \quad \dot{y}_i = v_i \sin\theta_i, \quad \dot{\theta}_i = \omega_i \tag{1}$$

where $\boldsymbol{q}_i = [x_i, y_i, \theta_i]^T \in \mathbb{R}^3$ denotes the pose of robot i in the global frame X-O-Y, and where $\boldsymbol{p}_i = [x_i, y_i]^T \in \mathbb{R}^2$ and $\theta_i \in (-\pi, \pi]$ denote its position and heading angle, respectively. $v_i \in \mathbb{R}$ and $\omega_i \in \mathbb{R}$ are its linear speed and angular speed, respectively. Considering the real linear and angular speed constraints, the speeds of robot i meet $v_i \in [-v_{\max}, v_{\max}]$ and $\omega_i \in [-\omega_{\max}, \omega_{\max}]$, where $v_{\max} \in \mathbb{R}^+$ and $\omega_{\max} \in \mathbb{R}^+$ are its maximum speed bounds.

Here, we assume the dynamics of a target as a single-integral model

$$\dot{\boldsymbol{p}}_0 = \boldsymbol{v}_0 \tag{2}$$

where $\boldsymbol{p}_0 = [x_0, y_0]^T \in \mathbb{R}^2$ and $\boldsymbol{v}_0 = [v_i^x, v_i^y]^T \in \mathbb{R}^2$ denote the position and speed of the target in the global frame, and v_i^x and v_i^y are the speeds of the target in the x and y directions, respectively.

Inspired by the related work [28], in this paper, we choose a bias point $\boldsymbol{p}_i{}' = [x_i{}', y_i{}']^T$ from the center point $\boldsymbol{p}_i$ of two wheels axis along the robot's orientation axis to distance d ($d \neq 0$), as shown in Figure 1. For this reason, we assume that the bias point can be placed in some distance or angle measurement sensors, such as Lidar, camera, and others, so that the measured date can be used directly without further conversion. In that case, the controller based on distance or angle information can be simply designed.

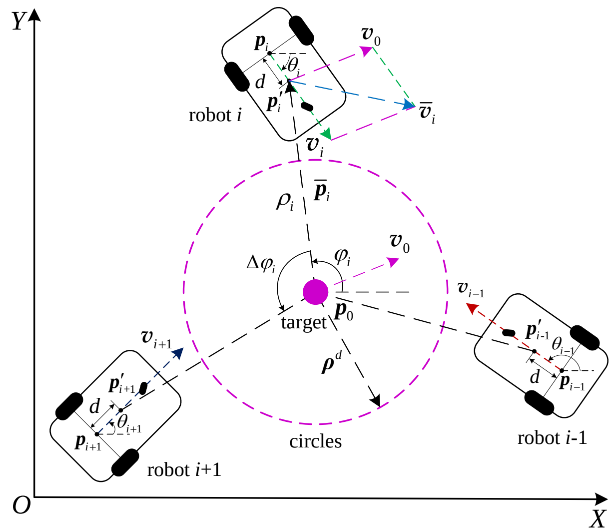

Figure 1. Illustration of the cooperative target enclosing.

Therefore, we consider to move the bias point $\boldsymbol{p}_i{}'$ into a circular formation instead of moving point $\boldsymbol{p}_i$, which has been studied in [29–32], and the bias point is defined as

$$\begin{bmatrix} x_i{}' \\ y_i{}' \end{bmatrix} = \begin{bmatrix} x_i \\ y_i \end{bmatrix} + d \begin{bmatrix} \cos\theta_i \\ \sin\theta_i \end{bmatrix} \tag{3}$$

The robot i is also described as a single-integral dynamics model

$$\dot{\boldsymbol{p}}_i' = \boldsymbol{u_i} \tag{4}$$

where $\boldsymbol{u}_i = [u_i^x, u_i^y]^T \in \mathbb{R}^2$ denotes the control input of robot i, and u_i^x and u_i^y are its control inputs in the x and y directions of the global frame, respectively.

Since the robots' motion is controlled directly by linear speed and angular speed or speeds of two driving wheels, it is necessary to transform the control input into the linear and angular speeds [20], which is given by

$$\begin{bmatrix} v_i \\ \omega_i \end{bmatrix} = \begin{bmatrix} \cos\theta_i & \sin\theta_i \\ -\frac{1}{d}\sin\theta_i & \frac{1}{d}\cos\theta_i \end{bmatrix} \begin{bmatrix} u_i^x \\ u_i^y \end{bmatrix} \tag{5}$$

In order to easily establish the mathematical model of the controller, we introduce the following variables. Let $\bar{\boldsymbol{p}}_i$ as the relative position between robot i and the target; it is expressed as follows

$$\bar{\boldsymbol{p}}_i = \boldsymbol{p}_i{}' - \boldsymbol{p}_0 \tag{6}$$

The relative velocity $\bar{\boldsymbol{v}}_i$ between robot i and the target can be described as follows:

$$\bar{\boldsymbol{v}}_i = \boldsymbol{v}_i{}' - \boldsymbol{v}_0 \tag{7}$$

where $\boldsymbol{v}_i = [v_i^x, v_i^y]^T \in \mathbb{R}^2$ denotes the velocity of robot i in the global frame and v_i^x and v_i^y are its speeds in the x and y directions, respectively.

Moreover, let $\rho_i = \|\bar{\boldsymbol{p}}_i\| > 0$, $\boldsymbol{\rho} = [\rho_1, \rho_2, ..., \rho_n]^T \in \mathbb{R}^n$. The phase angle of robot i with respect to the target is $\varphi_i \in (0, 2\pi]$, where it is also expressed as the orientation of the vector $\bar{\boldsymbol{p}}_i$. Then, denote $\Delta\varphi_i \in (0, 2\pi]$ as the relative angular spacing from robot i to robot $i+1$, and let $\Delta\boldsymbol{\varphi} = [\Delta\varphi_1, \Delta\varphi_2, \ldots, \Delta\varphi_n]^T \in \mathbb{R}^n$, complying with the following rules:

$$\Delta\varphi_i = \left\{ \begin{array}{ll} \varphi_{i+1} - \varphi_i, & i = 1, ..., n-1 \\ \varphi_1 - \varphi_n + 2\pi, & i = n \end{array} \right\} \quad (8)$$

Let $\Delta\boldsymbol{\varphi}^d = [\Delta\varphi_1^d, \Delta\varphi_2^d, ..., \Delta\varphi_n^d]^T \in \mathbb{R}^n$, where $\Delta\varphi_i^d$ is the desired relative angular spacing from robot i to robot i+1; $\boldsymbol{\rho}^d = [\rho_1^d, \rho_2^d, ..., \rho_n^d]^T \in \mathbb{R}^n$, where ρ_i^d is the desired relative distance between robot i and the target or the desired circle radius of robot i around the target. In addition, we usually denote φ_1^d as the desired initial phase of robot 1 on its circle. In that case, the circular formation can be described as $(\boldsymbol{\rho}^d, \Delta\boldsymbol{\varphi}^d, \varphi_1^d)$ if $\rho_i^d > 0$, $\Delta\varphi_i^d \in (0, 2\pi]$, $\varphi_1^d \in (0, 2\pi]$.

With the above preparation, we formulate the formation problems of interest as follows:

Question 1 (circular convergence). For a team of nonholonomic mobile robots with dynamics model (4) and a static or moving target with dynamics model (2), a circular motion control law is designed to make all robots converge to the desired relative distance $\boldsymbol{\rho}^d$ with the target, that is, $\lim_{t\to\infty} \boldsymbol{\rho}(t) = \boldsymbol{\rho}^d$.

Question 2 (phase positioning and spacing assignment). Under the condition that the target is encircled by a group of robots, a control law with custom angular spacing distribution between two adjacent robots and phase positioning is designed, so that the initial phase of each robot on its circle can be determined according to the prescribed relative angular spacing and the first robot's desired initial phase on its circle, that is, $\lim_{t\to\infty} \Delta\boldsymbol{\varphi}(t) = \Delta\boldsymbol{\varphi}^d$, $\lim_{t\to\infty} \varphi_1(t) = \varphi_1^d$.

Question 3 (obstacles avoidance). For a multi-robot system, there is a basic requirement to be able to effectively avoid obstacles. An obstacles avoidance control law needs to be designed for complicated environment changes, while ensuring the stability of the formation.

3. Controller Design

In this section, we propose a circular formation controller with obstacles avoidance composed of three coupled portions to solve above problems and provide rigorous theoretical proof. The structure of the designed controller scheme is shown in Figure 2, which will be described in more details below.

3.1. Circular Motion Control

We first propose a circular motion control law that guides each robot to converge to its own desired circle without considering phase angle and angular spacing on the circle. The design idea of this control scheme is that by rotating a fixed reference vector around the target point conterclockwise $\boldsymbol{p}_0$, a rotation change circular trajectory can be obtained. Then, the circular trajectory can be used as a reference value, and the robot tracks the reference value for circular motion. The control objective can be described as follows :

$$\bar{\boldsymbol{p}}_i(t) \to R(\phi_i(t))\vec{\boldsymbol{p}}_i(t_0)\rho_i^d, \quad t \to \infty \quad (9)$$

where $R(\phi_i(t)) \in \mathbb{R}^{2\times 2}$ is a rotation matrix of steering angle $\phi_i(t) \in (0, 2\pi]$ and $\vec{\boldsymbol{p}}_i(t_0)$ is the unit direction vector of $\bar{\boldsymbol{p}}_i(t_0)$ at the initial time t_0, which are defined as

$$\phi_i(t) = \varphi_i(t) - \varphi_i(t_0), \qquad t \geq t_0 \quad (10)$$

$$\vec{\boldsymbol{p}}_i(t_0) = \frac{\bar{\boldsymbol{p}}_i(t_0)}{\|\bar{\boldsymbol{p}}_i(t_0)\|} = \frac{\bar{\boldsymbol{p}}_i(t_0)}{\rho_i(t_0)} \tag{11}$$

$$\boldsymbol{R}(\phi_i(t)) = \begin{bmatrix} \cos\phi_i(t) & -\sin\phi_i(t) \\ \sin\phi_i(t) & \cos\phi_i(t) \end{bmatrix} \tag{12}$$

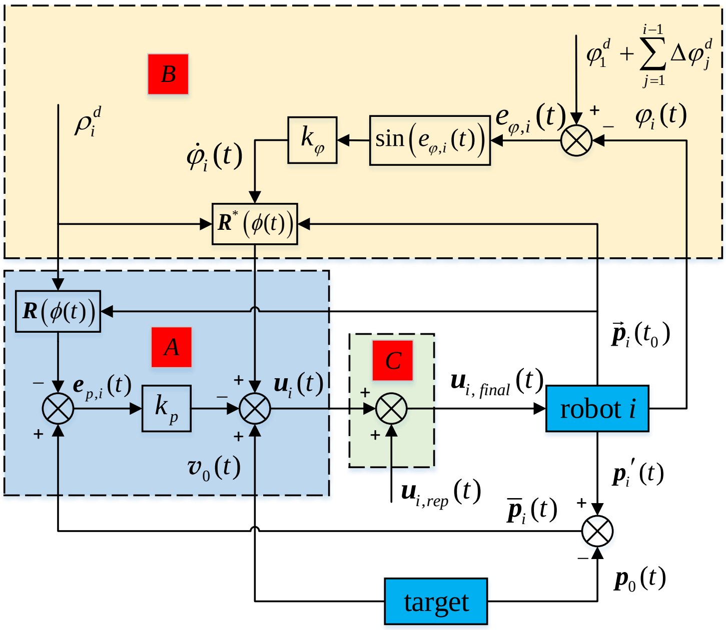

Figure 2. The structure of the designed controller scheme.

The circular motion control law is designed as follows:

$$\boldsymbol{u}_i(t) = \boldsymbol{v}_0(t) - k_p\left[\bar{\boldsymbol{p}}_i(t) - \boldsymbol{R}(\phi_i(t))\vec{\boldsymbol{p}}_i(t_0)\rho_i^d\right] + \dot{\boldsymbol{R}}(\phi_i(t))\vec{\boldsymbol{p}}_i(t_0)\rho_i^d \tag{13}$$

where k_p is a position constant, which is used to adjust the convergence speed of circular trajectory tracking for all robots.

Theorem 1. *Assuming $\phi_i(t)$ is a first-order continuous derivative function. Under the control law (13), robot i can converge to a circle with radius ρ_i^d centered on a static or moving target and maintain the set distance with the target, namely $\rho_i(t) \to \rho_i^d$ as $t \to \infty$.*

Proof . Denote the position error as

$$\boldsymbol{e}_{p,i}(t) = \bar{\boldsymbol{p}}_i(t) - \boldsymbol{R}(\phi_i(t))\vec{\boldsymbol{p}}_i(t_0)\rho_i^d \tag{14}$$

If (14) converges to zero, the error differential equation can be written as

$$\dot{\boldsymbol{e}}_{p,i}(t) = -k_p\boldsymbol{e}_{p,i}(t) \tag{15}$$

Substituting (6), (7) and (14) into (15) gives

$$\dot{\boldsymbol{p}}_i'(t) = \boldsymbol{v}_0(t) - k_p\left[\bar{\boldsymbol{p}}_i(t) - \boldsymbol{R}(\phi_i(t))\vec{\boldsymbol{p}}_i(t_0)\rho_i^d\right] + \dot{\boldsymbol{R}}(\phi_i(t))\vec{\boldsymbol{p}}_i(t_0)\rho_i^d \tag{16}$$

where

$$\dot{\boldsymbol{R}}(\phi_i(t)) = \dot{\phi}_i(t)\begin{bmatrix} -\sin\phi_i(t) & -\cos\phi_i(t) \\ \cos\phi_i(t) & -\sin\phi_i(t) \end{bmatrix} \tag{17}$$

According to the robot dynamics model (4), the controller (13) is obtained by (16). In addition, (15) can be solved as $\boldsymbol{e}_{p,i}(t) = \exp(-k_p t)\boldsymbol{e}_{p,i}(t_0)$. The position error $\boldsymbol{e}_{p,i}(t)$ could converge to $\mathbf{0}$ as $t \to \infty$ because of k_p as a positive constant and $\boldsymbol{e}_{p,i}(t_0)$ as a positive constant vector. So, the control objective (9) has been proved. Especially, when $\dot{\phi}_i(t) \neq 0$, all robots can rotate around the target uniformly. □

3.2. Custom Phasing and Spacing Control

Next, in order to ensure that the relative angular spacing between inter-robots is maintained within the desired values, the angular spacing of the desired formation can be carried out by changing the steering angles. According to (10), we can obtain $\dot{\phi}_i(t) = \dot{\varphi}_i(t)$. The control law (13) can be rewritten as

$$\boldsymbol{u}_i(t) = \boldsymbol{v}_0(t) - k_p\left[\bar{\boldsymbol{p}}_i(t) - \boldsymbol{R}(\phi_i(t))\vec{\boldsymbol{p}}_i(t_0)\rho_i^d\right] + \dot{\varphi}_i(t)\boldsymbol{R}^*(\phi_i(t))\vec{\boldsymbol{p}}_i(t_0)\rho_i^d \tag{18}$$

where,

$$\boldsymbol{R}^*(\phi_i(t)) = \begin{bmatrix} -\sin\phi_i(t) & -\cos\phi_i(t) \\ \cos\phi_i(t) & -\sin\phi_i(t) \end{bmatrix} \tag{19}$$

Considering the practical applications, it is sometimes necessary to determine the position of the robots on their own circles. For example, when a multi-robot system monitors an area of interest, the accurate position of each robot needs to be pre-planned to monitor a specific region. Therefore, it is necessary to design a phase positioning and spacing assignment control law, so that the robots can reach the specified position on their circles. We introduce a nonlinear function into the controller (18), which is described as follows:

$$\dot{\varphi}_i(t) = k_\varphi \sin\left[\left(\varphi_1^d + \sum_{j=1}^{i-1}\Delta\varphi_j^d\right) - \left(\varphi_1(t) + \sum_{j=1}^{i-1}\Delta\varphi_j(t)\right)\right] \tag{20}$$

where k_φ is a position constant, which is used to adjust the convergence speed of phase angle and angular spacing of the robots.

Theorem 2. *Under the circular motion control law (18), the phase positioning and spacing-assignment control law of all robots are satisfied (20). The phase angles of all robots on the circles can converge to the desired values calculated by desired initial phase φ_1^d of robot 1 and the desired relative angular spacing $\boldsymbol{\varphi}^d$, that is, $\lim\limits_{t\to\infty}\varphi_i(t) = \varphi_1^d + \sum\limits_{j=1}^{i-1}\Delta\varphi_j^d$ for $i = 1, 2, \cdots, n$, which contains two parts: the phase positioning convergence of the robot 1 , that is, $\lim\limits_{t\to\infty}\varphi_1(t) = \varphi_1^d$, and the relative angular spacing convergence of all robots , that is, $\lim\limits_{t\to\infty}\Delta\boldsymbol{\varphi}(t) = \Delta\boldsymbol{\varphi}^d$.*

Proof . Let $\varphi_i(t) = \varphi_1(t) + \sum\limits_{j=1}^{i-1}\Delta\varphi_j(t)$. We choose a positive definite Lyapunov function candidate

$$V = k_\varphi\left[1 - \cos\left(\varphi_1^d + \sum_{j=1}^{i-1}\Delta\varphi_j^d - \varphi_i(t)\right)\right] \tag{21}$$

Differentiating Equation (20) with respect to time as

$$\dot{V} = -k_\varphi \sin\left(\varphi_1^d + \sum_{j=1}^{i-1}\Delta\varphi_j^d - \varphi_i(t)\right)\dot{\varphi}_i(t) = -{k_\varphi}^2\sin^2\left(\varphi_1^d + \sum_{j=1}^{i-1}\Delta\varphi_j^d - \varphi_i(t)\right) \leq 0 \tag{22}$$

With (22), $\dot{V} \leq 0$ is guaranteed to be negative definite. Let $\dot{V} = 0$; there are the relative equilibrium points $\varphi_i(t) = \varphi_1^d + \sum_{j=1}^{i-1} \Delta\varphi_j^d$ for $i = 1, 2, ..., n$. This shows that the phase convergence of each robot is guaranteed by control laws (20).

To sum up, it is shown that the circular formation controller is demonstrated as stable by the control law (18) and (20). □

3.3. Obstacles Avoidance Control

Considering that the formation member will inevitably collide with obstacles in the environment and other members in the motion process, it is necessary to design an effective obstacle-avoidance control law that not only enables the robots to complete the barrier-void task but also ensures the stability of the formation. As a classical obstacle-avoidance control method, the artificial potential field method is widely used in robot's motion control. In the case discussed in this paper, it is not necessary to set up an additional attractive potential field function to generate attractive force because each robot has its own trajectory to track but only to set repulsive potential field to generate repulsive force for obstacles avoidance operation. The classical repulsive field function is defined as

$$\boldsymbol{U}_{i,rep}(t) = \begin{cases} \frac{1}{2}k_{rep} \sum\limits_{k=1}^{m} \left(\frac{1}{\rho_{i,obs}(t)} - \frac{1}{\rho_0} \right)^2, & \text{if } \rho_{i,obs}(t) \leq \rho_0 \\ 0, & \text{if } \rho_{i,obs}(t) > \rho_0 \end{cases} \tag{23}$$

where k_{rep} is a position constant, which is repulsion gain coefficient. $\rho_0 > 0$ is obstacle-avoidance response distance. $m \in \mathbb{N}$ is the number of obstacles in domain ρ_0. Denote $\boldsymbol{\rho}_{i,obs}(t) = \boldsymbol{p}_i{}'(t) - \boldsymbol{p}_{k,obs}(t)$, $\rho_{i,obs}(t) = \left\| \boldsymbol{\rho}_{i,obs}(t) \right\|$, where $\boldsymbol{p}_{k,obs}(t)$ is the position of obstacle k in the global frame.

Then, since repulsion force received by the robot is along the negative gradient of the repulsive field function, the obstacle-avoidance control law is expressed as follows:

$$\boldsymbol{u}_{i,rep}(t) = -\nabla \boldsymbol{U}_{i,rep}(t) = \begin{cases} k_{rep} \sum\limits_{k=1}^{m} \left(\frac{1}{\rho_{i,obs}(t)} - \frac{1}{\rho_0} \right) \frac{\boldsymbol{\rho}_{i,obs}(t)}{\rho_{i,obs}(t)^2}, & \text{if } \rho_{i,obs}(t) \leq \rho_0 \\ 0, & \text{if } \rho_{i,obs}(t) > \rho_0 \end{cases} \tag{24}$$

Finally, we combine (18), (20), and (24) to achieve circular formation control with obstacles avoidance, which can obtain the final control input of robot i as

$$\boldsymbol{u}_{i,final}(t) = \boldsymbol{u}_i(t) + \boldsymbol{u}_{i,rep}(t), \quad i = 1, 2, ..., n \tag{25}$$

By substituting (25) into (5), the linear and angular speeds of all robots in the circular formation can be obtained.

4. Simulation and Experimental Results

In this section, we verify the feasibility and effectiveness of the designed circular formation controller with obstacles avoidance through simulations and experiments. We first use MATLAB R2018b platform to carry out numerical simulations. Then, we utilize three nonholonomic mobile robots based on Ubuntu 18.04 with ROS (Robot Operating System) to further verify the performance of the proposed controller.

4.1. Simulations

In the numerical simulations, a multi-robot system consisting of five nonholonomic mobile robots represented by kinematic points with direction is considered, and their initial poses are generated randomly in a plane. A target remains stationary or in motion state, and its initial position is the point (1.5, −1.5) in the global frame. Meanwhile, some obstacles are randomly placed in the plane. In this part, we will consider three cases: a target in static state for case 1, a moving target with constant speed for case 2, and a moving target with time-varying speed for case 3. The three typical motion state of the target are simulated and tested, which are shown in Figures 3–5. In addition, parameters of three groups of simulations are shown in Table 1.

Table 1. The parameters of three groups of simulations.

Parameter	Case 1	Case 2	Case 3	Unit
$\boldsymbol{\rho}^d$	$[0.9, 0.6, 0.9, 1.2, 0.9]^T$	$[1, 1, 1, 1, 1]^T$	$[1.5, 1, 1.5, 1.5, 1]^T$	m
$\Delta\boldsymbol{\varphi}^d$	$[-\pi/2, \pi, \pi/3, \pi/3, 5\pi/6]^T$	$[2\pi/5, 2\pi/5, 2\pi/5, 2\pi/5, 2\pi/5]^T$	$[\pi/2, \pi/3, \pi/3, \pi/3, \pi/2]^T$	rad
φ_1^d	$\pi/2$	0	$\pi/3$	rad
d	0.1	0.1	0.1	m
ρ_0	0.5	0.5	0.5	m
k_p	0.3	0.5	0.5	—
k_φ	0.3	0.5	0.5	—
k_{rep}	0.2	0.3	0.3	—

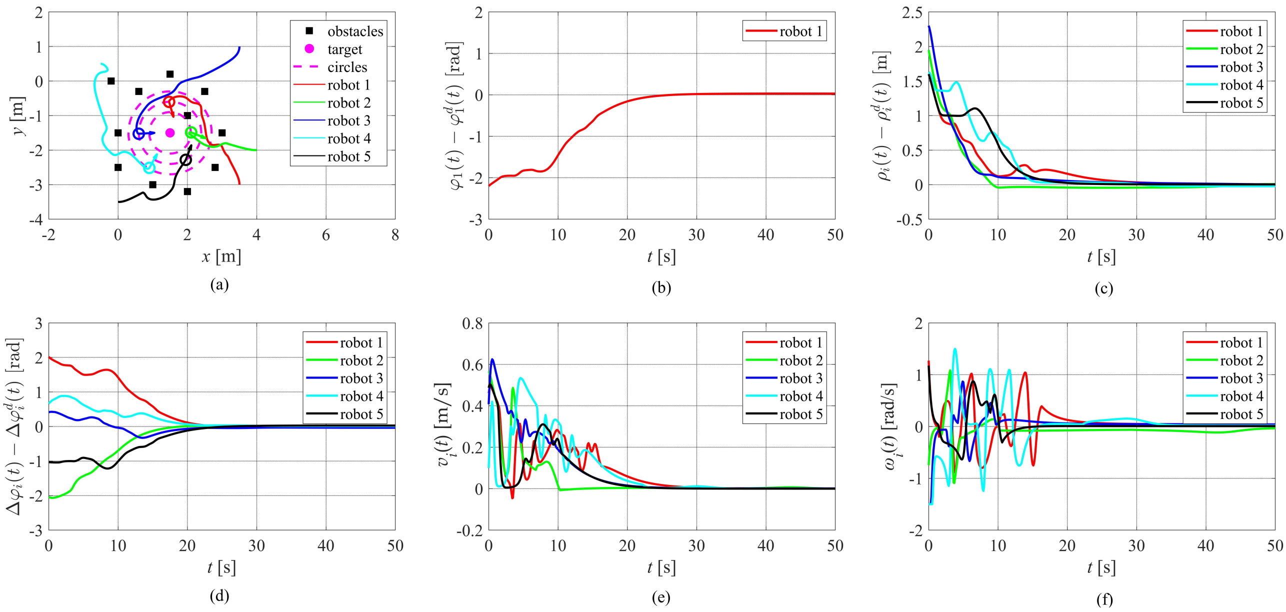

Figure 3. Simulation results of case 1. (**a**) Trajectories of five robots and a static target in a plane. (**b**) Error between current phase and the desired phase of robot 1. (**c**) Distance errors between five robots and their desired circles centered on the target. (**d**) Errors between current angular spacing and the desired angular spacing of all adjacent inter-robots. (**e**) The linear speeds of five robots. (**f**) The angular speeds of five robots.

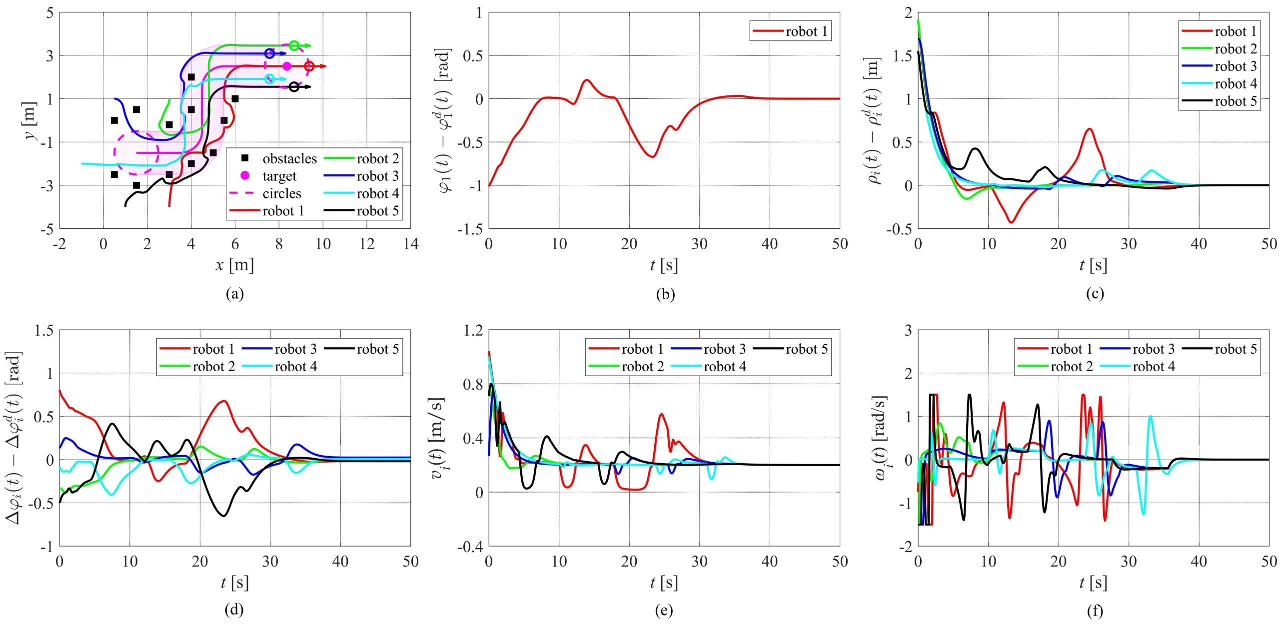

Figure 4. Simulation results of case 2. (**a**) Trajectories of five robots and a moving target with a constant speed in a plane. (**b**) Error between current phase and the desired phase of robot 1. (**c**) Distance errors between five robots and their desired circles centered on the target. (**d**) Errors between current angular spacing and the desired angular spacing of all adjacent inter-robots. (**e**) The linear speeds of five robots. (**f**) The angular speeds of five robots.

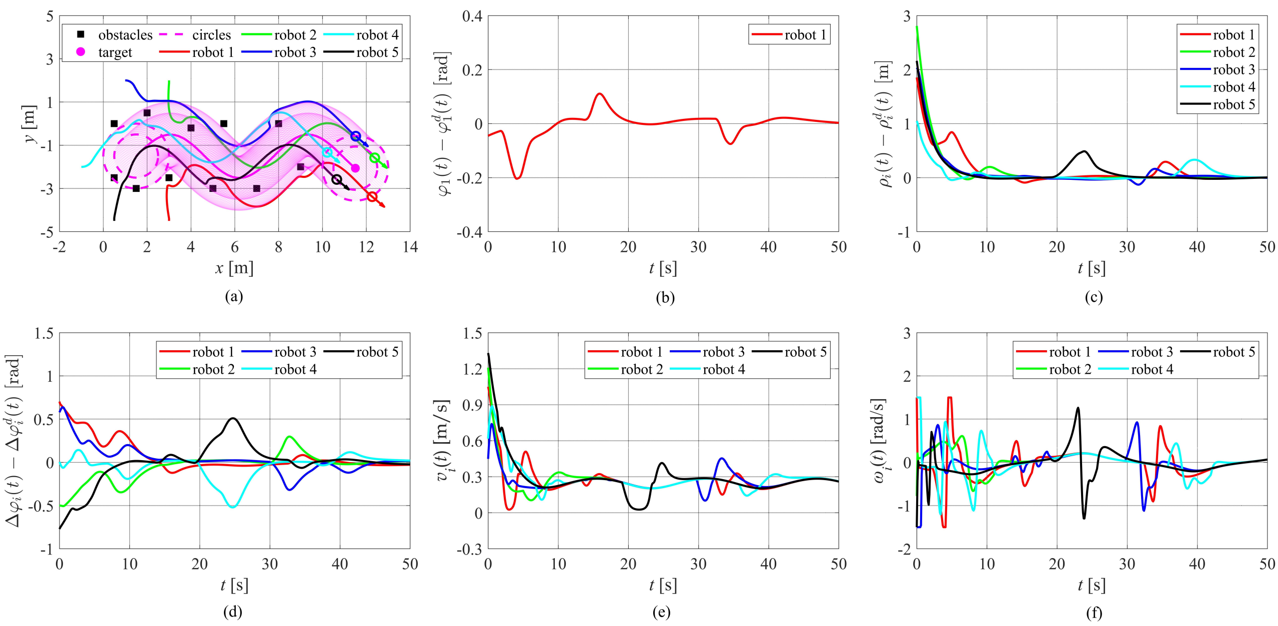

Figure 5. Simulation results of case 3. (**a**) Trajectories of five robots and a moving target with time-varying speed in a plane. (**b**) Error between current phase and the desired phase of robot 1. (**c**) Distance errors between five robots and their desired circles centered on the target. (**d**) Errors between current angular spacing and the desired angular spacing of all adjacent inter-robots. (**e**) The linear speeds of five robots. (**f**) The angular speeds of five robots.

4.1.1. Case 1 (A Static Target)

In case 1, the initial poses of five robots and the speed of the target are, respectively, $\boldsymbol{q}_1(0) = [3.5, -3, \pi/2]^T$, $\boldsymbol{q}_2(0) = [4, -2, \pi]^T$, $\boldsymbol{q}_3(0) = [3.5, 1, -\pi/2]^T$, $\boldsymbol{q}_4(0) = [-0.5, 0.5, 0]^T$, $\boldsymbol{q}_5(0) = [0, -3.5, 0]^T$, $\boldsymbol{v}_0(t) = [0, 0]^T$.

The motion trajectories from Figure 3a show that the robots can form desired circular formation with three different circles radii and four different angular spacings, and avoid obstacles effectively. Moreover, it can be seen from Figure 3b–d that the initial phase of robot 1 on its circle, the relative distance between the robots and the target, and the angular spacing between the adjacent robots can converge to the desired values. In addition, the output linear and angular speeds of the designed controller from Figure 3e,f can meet the actual speed requirements of the robots, and the maximum linear and angular speeds of the robots are set to $v_{\max} = 1.5$ m/s and $\omega_{\max} = 1.5$ rad/s in order to prevent excessive input speeds.

4.1.2. Case 2 (A Moving Target with a Constant Speed)

In case 2, the initial poses of five robots are, respectively, $\boldsymbol{q}_1(0) = [3, -4, \pi/2]^T$, $\boldsymbol{q}_2(0) = [3, 1, -\pi/2]^T$, $\boldsymbol{q}_3(0) = [0.5, 1, 0]^T$, $\boldsymbol{q}_4(0) = [-1, -2, 0]^T$, $\boldsymbol{q}_5(0) = [1, -4, \pi/2]^T$, and the speeds of the target are set to $v_0^x(t) = 0.2$, $v_0^y(t) = 0$ for $t \leq 10$ s; $v_0^x(t) = 0.2\cos(0.2(t-10))$, $v_0^y(t) = 0.2\sin(0.2(t-10))$ for 10 s $< t \leq (10 + 2.5\pi)$ s; $v_0^x(t) = 0$, $v_0^y(t) = 0.2$ for $(10 + 2.5\pi)$ s $< t \leq (20 + 2.5\pi)$ s; $v_0^x(t) = 0.2\sin(0.2(t - 20 - 2.5\pi))$, $v_0^y(t) = 0.2\cos(0.2(t - 20 - 2.5\pi))$ for $(20 + 2.5\pi)$ s $< t \leq (20 + 5\pi)$ s; $v_0^x(t) = 0.2$, $v_0^y(t) = 0$ for $(20 + 5\pi)$ s $< t \leq 50$ s. The linear speed of the moving target is a constant value, i.e., $\|\boldsymbol{v}_0(t)\| = 0.2$ m/s. It can be seen from Figure 4a–d that the five robots can track the moving target with a constant speed and evenly form a desired circular formation with expected $\boldsymbol{\rho}^d$, $\Delta\boldsymbol{\varphi}^d$ and φ_1^d, and can avoid obstacles in real time. Figure 4e also shows that the linear speeds of the robots converge to the linear speed of the target.

4.1.3. Case 3 (A Moving Target with Time-Varying Speed)

In case 3, the initial poses of five robots and the speed of the target are respectively $\boldsymbol{q}_1(0) = [3, -4.5, \pi/2]^T$, $\boldsymbol{q}_2(0) = [3, 2, -\pi/2]^T$, $\boldsymbol{q}_3(0) = [1, 2, 0]^T$, $\boldsymbol{q}_4(0) = [-1, -2, 0]^T$, $\boldsymbol{q}_5(0) = [0.5, -4.5, \pi/2]^T$, $\boldsymbol{v}_0(t) = [0.2, 0.2\cos(0.2t)]^T$.

The linear speed of the moving target is time-varying value, which presents sine curve variation. It can be seen from Figure 5a that the five robots can form the desired circular formation with two different circle radii as well as two different angular spacings and implement obstacles avoidance effectively in the moving conditions. Figure 5b–d illustrate that the tracking errors of the forming circular formation converge to zero, which has good performance. In addition, Figure 5e,f also illustrate that the linear and angular speeds of the robots under speed constraints converge to the speeds of the target.

To sum up, the above three groups of simulation results show that the multi-robot system can achieve desired control objectives. The position errors between the robots and the target, as well as the angular spacing errors between inter-robots, fluctuate when the robots detect the obstacles, and the errors converge to zero after leaving the obstacles. In addition, the output speeds of the controller is within a reasonable range.

4.2. Experiments

4.2.1. Experiments Platform

In the experiments, three nonholonomic mobile robots are taken as the research objectives, and the experimental platform of the multi-robot system is shown in Figure 6. The three robots and a computer are in the same WLAN (Wireless Local Area Network), which can realize the communication between inter-robots and computer. The odometry data of the robots is obtained by the AB phase photoelectric encoder of the DC (Direct-Current) motor with a high-resolution of 500 lines/laps, and then real-time poses of the robots are obtained by EKF (Extended Kalman Filter) fusion algorithm with the IMU (Inertial Measurement Unit) data. The Lidar that is placed at the bias point obtains the distance information between the robot and obstacles. We take the poses information as well as the distance information as the inputs of our proposed controller, calculate the linear and angular speeds of the robots in real time, and finally convert them into the speeds of the DC motor of the left and right driving wheels to realize the movement of the robots.

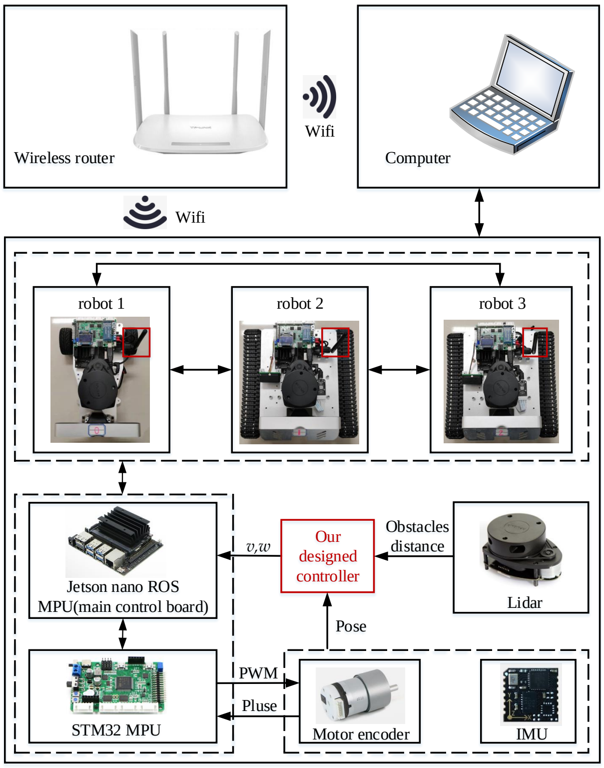

Figure 6. Multiple nonholonomic mobile robots experiment platform.

4.2.2. Multi-Mobile Robot Experiments

Just like the simulations, we also carried out our approach in three cases. Referring to the simulations for the initial position and speed of the target, other parameters of three groups of experiments are shown in Table 2. The experimental results are shown in Figures 7–9. The motion trajectories in Figures 7a,b–9a,b indicate that the three nonholonomic mobile robots can track a stationary or moving target, form a uniformly distributed circular formation with the same or different radii around the target, and effectively avoid the obstacles encountered. Figures 7c–e and 8c–e indicate that the errors of the control objectives fluctuate around zero, but Figure 9c,e show that the phase error of robot 1 and the angular spacing error between the each pair of two adjacent robots fluctuate greatly because of the angular speed of the target is always fluctuating. It takes a certain time to adjust the robots' orientation to achieve the desired values, as can be seen from the output angular speed of the controller in Figure 9g. However, it can be seen from Figure 9f that all robots can track the linear speed of the target.

The above three groups of experiments can obtain similar results to the simulations, which shows that the designed controller can work effectively and perform well.

Table 2. The parameters of three groups of experiments.

Parameter	Case 1	Case 2	Case 3	Unit
$\boldsymbol{\rho}^d$	$[0.8, 0.8, 1.2]^T$	$[0.5, 0.5, 0.5]^T$	$[0.5, 0.5, 0.5]^T$	m
$\Delta\boldsymbol{\varphi}^d$	$[2\pi/3, 2\pi/3, 2\pi/3]^T$	$[2\pi/3, 2\pi/3, 2\pi/3]^T$	$[2\pi/3, 2\pi/3, 2\pi/3]^T$	rad
φ_1^d	$\pi/2$	0	0	rad
d	0.1	0.1	0.1	m
ρ_0	0.65	0.65	0.65	m
k_p	0.2	0.2	0.2	—
k_φ	0.3	0.3	0.3	—
k_{rep}	0.3	0.3	0.3	—

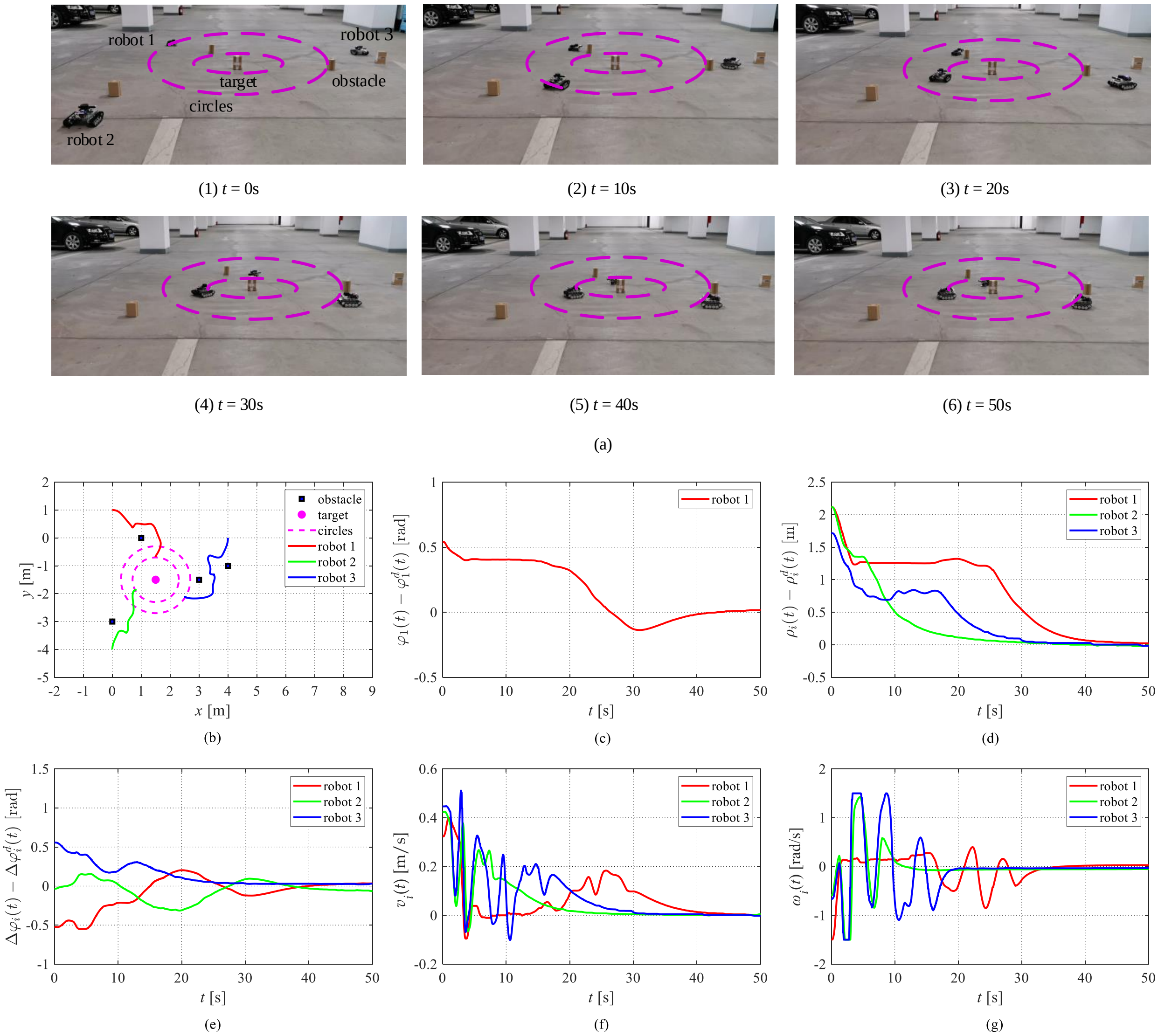

Figure 7. Experimental results of case 1. (**a**) The motion views of three nonholonomic mobile robots forming a evenly distributed circular formation with two different circular radii to enclose a static target. (**b**) Trajectories of the three robots and the target in the plane. (**c**) Error between current phase and the desired phase of robot 1. (**d**) Distance errors between the three robots and their desired circles centered on the target. (**e**) Errors between current angular spacing and the desired angular spacing of all adjacent inter-robots. (**f**) The linear speeds of the three robots. (**g**) The angular speeds of the three robots.

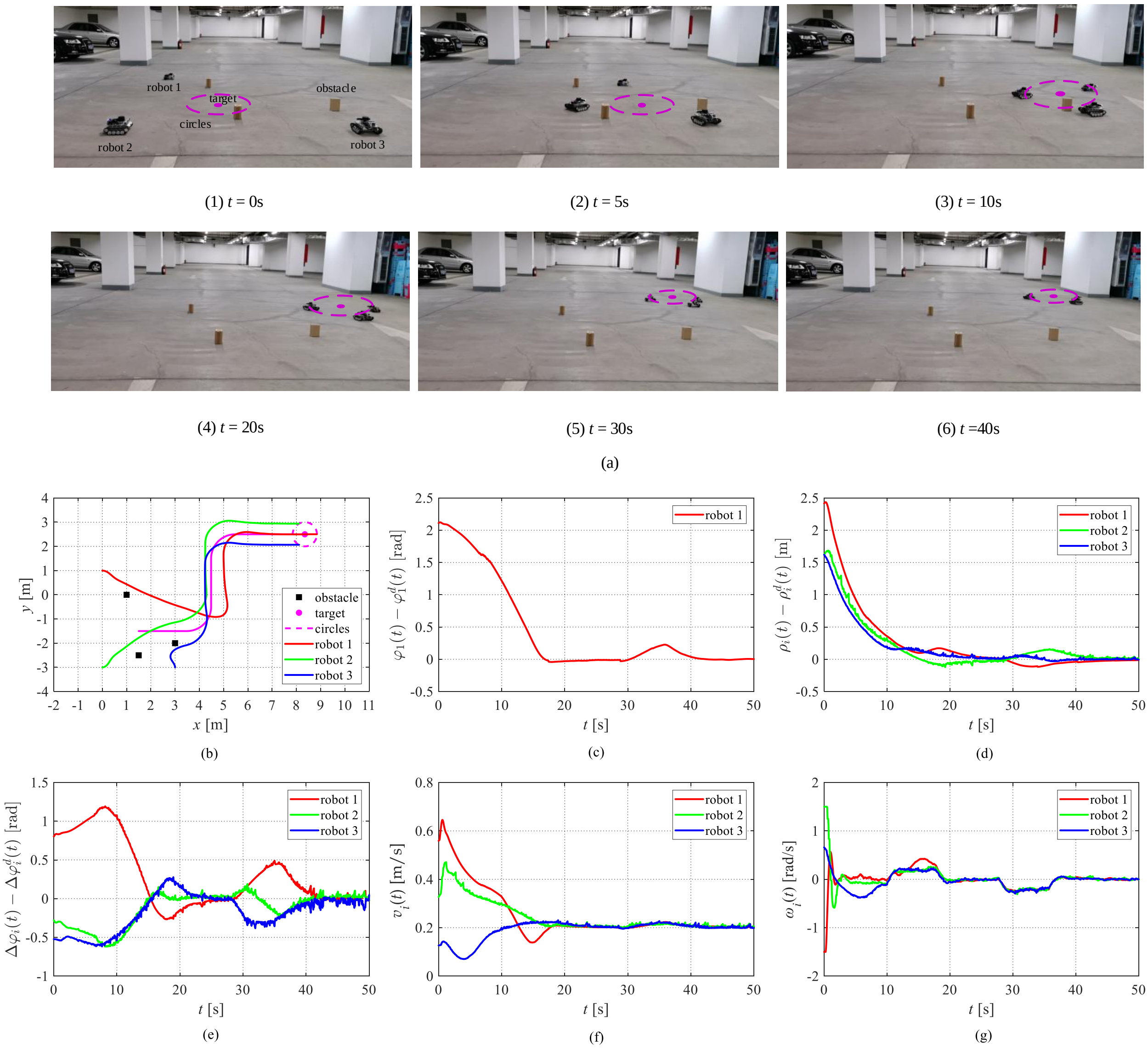

Figure 8. Experimental results of case 2. (**a**) The motion views of three nonholonomic mobile robots forming a evenly distributed circular formation with same circular radius to enclose and track a moving target with a constant speed. (**b**) Trajectories of the three robots and the target in the plane. (**c**) Error between current phase and the desired phase of robot 1. (**d**) Distance errors between the three robots and their desired circles centered on the target. (**e**) Errors between current angular spacing and the desired angular spacing of all adjacent inter-robots. (**f**) The linear speeds of the three robots. (**g**) The angular speeds of the three robots.

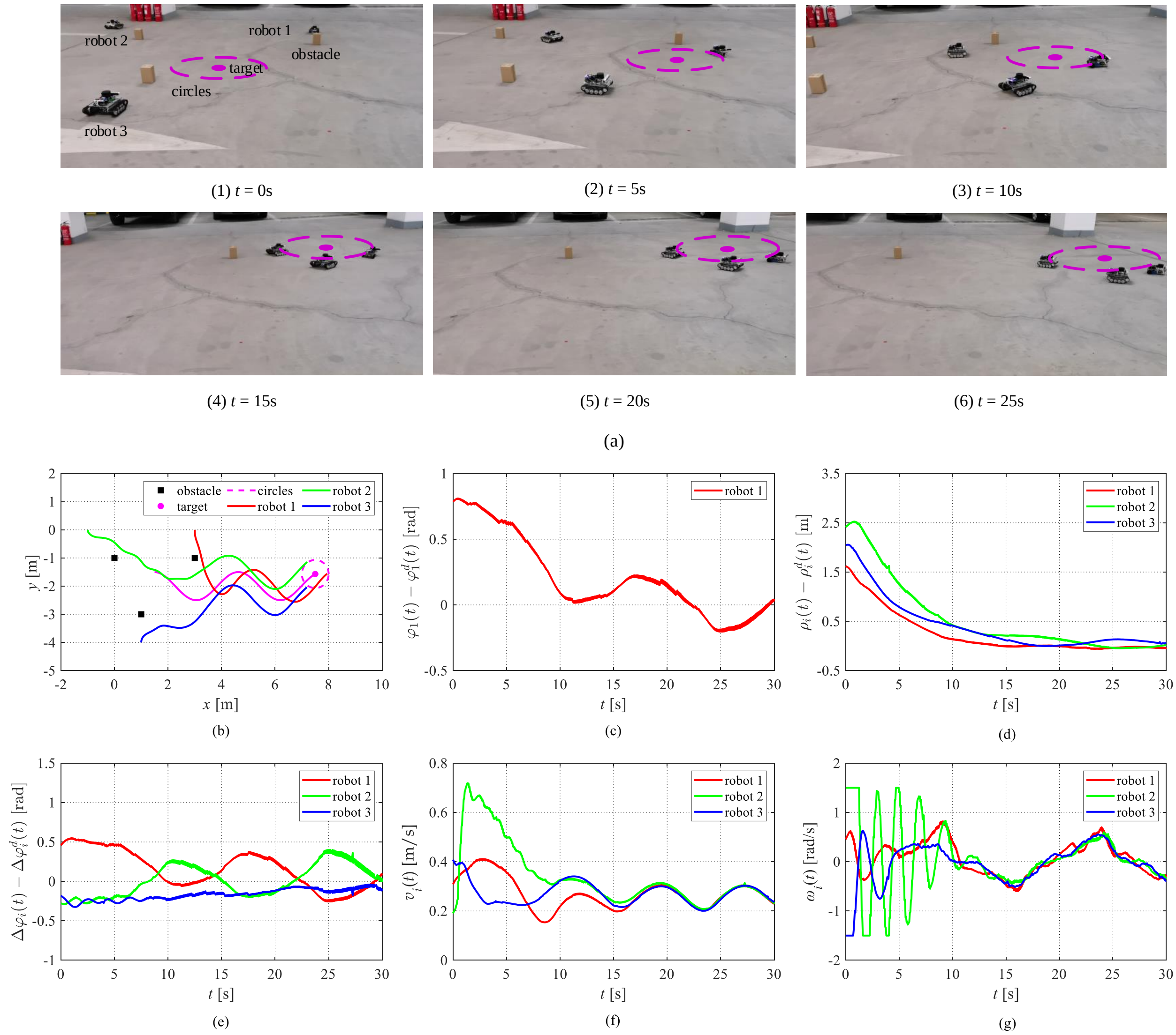

Figure 9. Experimental results of case 3. (**a**) The motion views of three nonholonomic mobile robots forming a evenly distributed circular formation with same circular radius to enclose and track a moving target with time-varying speed. (**b**) Trajectories of the three robots and the target in the plane. (**c**) Error between current phase and the desired phase of robot 1. (**d**) Distance errors between the three robots and their desired circles centered on the target. (**e**) Errors between current angular spacing and the desired angular spacing of all adjacent inter-robots. (**f**) The linear speeds of the three robots. (**g**) The angular speeds of the three robots.

5. Conclusions

In this paper, we have proposed a circular formation controller with obstacles avoidance for a group of multiple nonholonomic mobile robots to collaboratively encircle and track a static or moving target in an environment with obstacles. The controller includes three sub-parts, where the first is circular motion control law by using the idea of circular trajectory tracking control that each robot moves to the desired circular around a target, maintaining a preset distance between the robots and the target; the second is phase positioning and spacing assignment control law by introducing a nonlinear function, for which each robot can determine the initial phase on the circle itself and maintain the desired relative angular spacing from its neighbors; and the third is obstacle-avoidance control law, which only considers the repulsive potential field, for which each robot is able to effectively avoid obstacles in the complicated environment while maintaining the stability of the formation. Then, theoretical analysis has been provided to show the convergence of the system under the proposed controller. Finally, the simulation and experimental results demonstrate good control performance of the proposed control scheme. The controller can realize multiple nonholonomic mobile robots with speed constrains fencing around and tracking a static or moving target in an environment with obstacles, which has great practical value for engineering applications.

In future work, our proposed control scheme should be implemented in a local frame that is more in line with practical engineering so that only local information is utilized without knowing global information. In addition, the position and velocity of the target are difficult to obtain directly in practice, especially in the global frame. It is necessary to design an estimation law so that each robot can estimate the position and velocity of the target.

Author Contributions: Conceptualization, X.L. (Xinghua Li) and S.H.; Data curation, X.L. (Xiaoping Liu); Formal analysis, G.W.; Funding acquisition, G.W.; Investigation, S.H.; Methodology, X.L. (Xinghua Li) and G.W.; Project administration, G.W.; Resources, X.L. (Xiaoping Liu); Software, X.L. (Xinghua Li); Validation, X.L. (Xiaoping Liu), G.W., C.S. and H.C.; Writing—original draft, X.L. (Xinghua Li); Writing—review and editing, X.L. (Xinghua Li). All authors have read and agreed to the published version of the manuscript.

Funding: This research was funded by the Science and Technology Project of Fire and Rescue Bureau of Emergency Management Department, Grant No. 2020XFZD15.

Institutional Review Board Statement: Not applicable.

Informed Consent Statement: Not applicable.

Data Availability Statement: Not applicable.

Acknowledgments: We would like to thank Beijing University of Posts and Telecommunications for providing the experimental site and the cooperative unit China Academy of Safety Science and Technology for providing project funds.

Conflicts of Interest: We declare that we have no financial and personal relationships with other people or organizations that can inappropriately influence our work, there is no professional or other personal interest of any nature or kind in any product, service and/or company that could be construed as influencing the position presented in, or the review of, the manuscript entitled, "Cooperative Target Enclosing and Tracking Control with Obstacles Avoidance for Multiple Nonholonomic Mobile Robots".

References

1. Koung, D.; Kermorgant, O.; Fantoni, I.; Belouaer, L. Cooperative multi-robot object transportation system based on hierarchical quadratic programming. *IEEE Robot. Autom. Lett.* **2021**, *6*, 6466–6472. [CrossRef]
2. Choi, D.; Kim, D. Intelligent multi-robot system for collaborative object transportation tasks in rough terrains. *Electronics* **2021**, *10*, 1499. [CrossRef]
3. Mas, I.; Li, S.; Acain, J.; Kitts, C. Entrapment/escorting and patrolling missions in multi-robot cluster space control. In Proceedings of the IEEE/RSJ International Conference on Intelligent Robots and Systems, St. Louis, MO, USA, 10–15 October 2009.
4. Xie, J.; Zhou, R.; Luo, J.; Peng, Y.; Pu, H. Hybrid partition-based patrolling scheme for maritime area patrol with multiple cooperative unmanned surface vehicles. *J. Mar. Sci. Eng.* **2020**, *8*, 936–950. [CrossRef]
5. Schlanbusch, R.; Kristiansen, R.; Nicklasson, P.J. Spacecraft formation reconfiguration with collision avoidance. *Automatica* **2011**, *47*, 1443–1449. [CrossRef]
6. Yao, W.; Lu, H.; Zeng, Z.; Xiao, Z.; Zheng, Z. Distributed static and dynamic circumnavigation control with arbitrary spacings for a heterogeneous multi-robot system. *J. Intell. Robot. Syst.* **2019**, *94*, 883–905. [CrossRef]
7. Macwan, A.; Vilela, J.; Nejat, G.; Benhabib, B. A multirobot path-planning strategy for autonomous wilderness search and rescue. *IEEE Trans. Cybern.* **2015**, *45*, 1784–1797. [CrossRef]
8. Robin, C.; Lacroix, S. Multi-robot target detection and tracking: Taxonomy and survey. *Auton. Robot.* **2015**, *40*, 729–760. [CrossRef]
9. Kim, T.H. Cooperative control for target-capturing task based on a cyclic pursuit strategy. *Automatica* **2007**, *43*, 1426–1431. [CrossRef]
10. Fargeas, J.L.; Kabamba, P.; Girard, A. Cooperative surveillance and pursuit using unmanned aerial vehicles and unattended ground sensors. *Sensors* **2015**, *15*, 1365–1388. [CrossRef]
11. Leonard, N.E.; Paley, D.A.; Lekien, F.; Sepulchre, R.; Fratantoni, D.M.; Davis, R.E. Collective motion, sensor networks, and ocean sampling. *Proc. IEEE* **2007**, *95*, 48–74. [CrossRef]

12. Beard, R.W.; McLain, T.W.; Nelson, D.B.; Kingston, D.; Johanson, D. Decentralized cooperative aerial surveillance using fixed-wing miniature UAVs. *Proc. IEEE* **2006**, *94*, 1306–1324. [CrossRef]
13. Zhang, J.; Sha, J.; Han, G.; Liu, J.; Qian, Y. A cooperative-control-based underwater target escorting mechanism with multiple autonomous underwater vehicles for underwater Internet of Things. *IEEE Internet Things J.* **2020**, *8*, 4403–4416. [CrossRef]
14. Chen, W.; Zhou, S.; Pan, Z.; Zheng, H.; Liu, Y. Mapless collaborative navigation for a multi-robot system based on the deep reinforcement learning. *Appl. Sci.* **2019**, *9*, 4198. [CrossRef]
15. Kou, L.; Huang, Y.; Chen, Z.; He, S.; Xiang, J. Cooperative fencing control of multiple second-order vehicles for a moving target with and without velocity measurements. *Int. J. Robust Nonlinear Control* **2021**, *31*, 4602–4615. [CrossRef]
16. Huo, M.; Duan, H.; Fan, Y. Pigeon-inspired circular formation control for multi-uav system with limited target information. *Guid. Navig. Control* **2021**, *1*, 2150003. [CrossRef]
17. Zhang, C.; Li, Y.; Qi, G.; Sheng, A. Distributed finite-time control for coordinated circumnavigation with multiple agents under directed topology. *J. Frankl. Inst.* **2020**, *357*, 11710–11729. [CrossRef]
18. Shames, I.; Dasgupta, S.; Fidan, B.; Anderson, B.D.O. Circumnavigation using distance measurements under slow drift. *IEEE Trans. Autom. Control* **2012**, *57*, 889–903. [CrossRef]
19. Deghat, M.; Davis, E.; See, T.; Shames, I.; Anderson, B.D.O.; Yu, C. Target localization and circumnavigation by a non-holonomic robot. In Proceedings of the IEEE/RSJ International Conference on Intelligent Robots and Systems, Vilamoura-Algarve, Portugal, 7–12 October 2012.
20. Zheng, R.; Liu, Y.; Sun, D. Enclosing a target by nonholonomic mobile robots with bearing-only measurements. *Automatica* **2015**, *53*, 400–407. [CrossRef]
21. Yu, X.; Liu, L. Cooperative control for moving-target circular formation of nonholonomic vehicles. *IEEE Trans. Autom. Control* **2017**, *62*, 3448–3454. [CrossRef]
22. Miao, Z.; Wang, Y.; Fierro, R. Cooperative circumnavigation of a moving target with multiple nonholonomic robots using backstepping design. *Syst. Control Lett.* **2017**, *103*, 58–65. [CrossRef]
23. Wang, C.; Xie, G.; Cao, M. Forming circle formations of anonymous mobile agents with order preservation. *IEEE Trans. Autom. Contr.* **2013**, *58*, 3248–3254. [CrossRef]
24. Wang, C.; Xie, G. Limit-cycle-based design of formation control for mobile agents. *IEEE Trans. Autom. Control* **2019**, *65*, 3530–3543. [CrossRef]
25. Antonelli, G.; Arrichiello, F.; Chiaverini, S. The entrapment/escorting mission for a multi-robotsystem: Theory and experiments. In Proceedings of the IEEE/ASME International Conference on Advanced Intelligent Mechatronics, Zurich, Switzerland, 4–7 September 2007.
26. Arrichiello, F.; Chiaverini, S.; Indiveri, G.; Pedone, P. The null-space based behavioral control for a team of cooperative mobile robots with actuator saturations. In Proceedings of the IEEE/RSJ International Conference on Intelligent Robots and Systems, St. Louis, MO, USA, 10–15 October 2009.
27. Gao, S.; Song, R.; Li, Y. Coordinated control of multiple Euler–Lagrange systems for escorting missions with obstacle avoidance. *J. Appl. Sci.* **2019**, *9*, 4144–4166. [CrossRef]
28. Peng, X.; Guo, K.; Li, X.; Geng, Z. Cooperative moving-target enclosing control for multiple nonholonomic vehicles using feedback linearization approach. *IEEE Trans. Syst. Man Cybern.* **2019**, *51*, 4929–4935. [CrossRef]
29. Zhang, C.; Li, Y.; Qi, G.; Sheng, A. Distributed finite-time control for coordinated circumnavigation with multiple non-holonomic robots. *Nonlinear Dyn.* **2019**, *98*, 573–588. [CrossRef]
30. Yu, X.; Ding, N.; Zhang, A.; Qian, H. Cooperative moving-target enclosing of networked vehicles with constant linear velocities. *IEEE Trans. Cybern.* **2020**, *50*, 798–809. [CrossRef]
31. Brinon-Arranz, L.; Seuret, A.; Canudas-De-Wit, C. Cooperative control design for time-varying formations of multi-agent systems. *IEEE Trans. Autom. Control* **2014**, *59*, 2283–2288. [CrossRef]
32. Guo, J.; Yan, G.; Lin, Z. Local control strategy for moving-target-enclosing under dynamically changing network topology. *Syst. Control Lett.* **2010**, *59*, 654–661. [CrossRef]